

Supplementary Information - Atomic clock transitions in silicon-based spin qubits

Gary Wolfowicz,* Alexei M. Tyryshkin, Richard E. George, Helge Riemann, Nikolai V. Abrosimov, Peter Becker, Hans-Joachim Pohl, Mike L. W. Thewalt, Stephen A. Lyon, and John J. L. Morton[†]

S1. ESR- AND NMR-TYPE MAGNETIC FIELD “CLOCK” TRANSITIONS (CT)

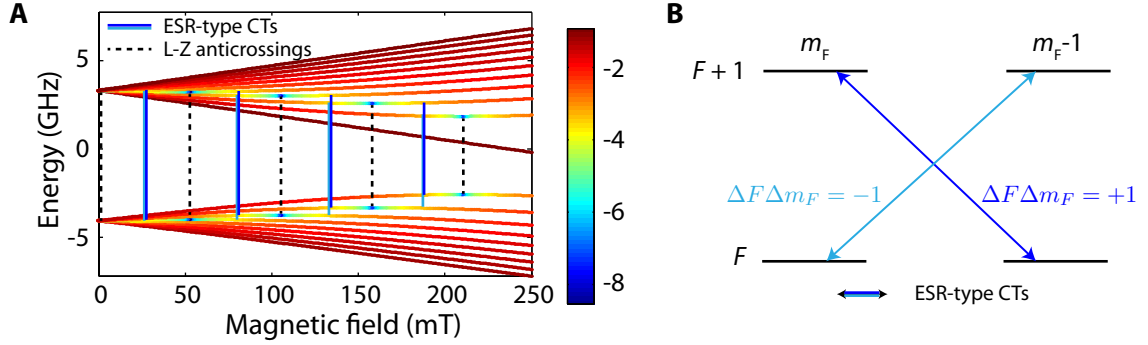


FIG. 1. **Description of ESR-type CTs.** **A**, The eigenstate energies of Si:Bi as function of magnetic field. The color scale shows the logarithmic distance to pure Bell states (Landau-Zener (L-Z) anticrossings) in the $|m_S, m_I\rangle$ basis, defined as $\log(|\theta - \pi/4|)$ for an eigenstate $|\Phi\rangle = \cos(\theta) |\mp\frac{1}{2}, m_I \pm \frac{1}{2}\rangle \pm \sin(\theta) |\pm\frac{1}{2}, m_I \mp \frac{1}{2}\rangle$. The Bell state at 0 mT is barely visible here due to degeneracy. **B**, ESR-type CTs with $\Delta F \Delta m_F = +1$ in dark blue and -1 in light blue. The four involved eigenstates, which are two pairs of hyperfine coupled states in the $|m_S, m_I\rangle$ basis, form a subspace of the Hilbert space.

Below we discuss the general requirements for ESR and NMR-type CTs for systems with electron spin $S = 1/2$ and nuclear spin I and assuming an isotropic hyperfine coupling, with a particular focus on Group V donors in silicon. This letter is the first measurement of ESR-type CTs to our knowledge, though they have been theoretically described by Mohammady *et.al.* [1, 2] for donors in Si, in particular Bi. On the other hand, NMR-type CTs have been used in various systems in the past [3, 4], including in phosphorus donors in silicon [5], to reduce sensitivity to magnetic field inhomogeneities (i.e. increase frequency resolution) or to increase nuclear coherence times.

In the basis of the electron and nuclear spin $|m_S, m_I\rangle$, the isotropic hyperfine interaction $(A\vec{I} \cdot \vec{S})$ couples pairs of states within the Hilbert space such that $[\Delta m_S = \pm 1, \Delta m_I = \mp 1]$. In the strongly coupled electron-nuclear spin basis $|F, m_F\rangle$ ($F = I \pm S, m_F = m_S + m_I$), these pairs of states share the same m_F value. When the static magnetic field is increased, the Zeeman energy rises to the same order of magnitude as the hyperfine interaction, resulting in avoided Landau-Zener crossings between states with $m_F \leq 0$ as shown in Figure 1A. ESR-type CTs are located between pairs of these avoided crossings.

At the intermediate fields relevant to CTs and Landau-Zener anticrossing, the eigenstates can be expressed either as being close to Bell states in the $|m_S, m_I\rangle$ basis, or still quite pure in the $|F, m_F\rangle$ basis. For example, the CT at 7.0317 GHz, explored in the main text, connects the following pairs of states:

$$-0.74 \left| \frac{1}{2}, -\frac{5}{2} \right\rangle + 0.67 \left| -\frac{1}{2}, -\frac{3}{2} \right\rangle \Leftrightarrow 0.74 \left| \frac{1}{2}, -\frac{3}{2} \right\rangle + 0.67 \left| -\frac{1}{2}, -\frac{1}{2} \right\rangle \quad \text{in the } |m_S, m_I\rangle \text{ basis}$$

$$0.99 |4, -2\rangle + 0.15 |5, -2\rangle \Leftrightarrow -0.15 |4, -1\rangle + 0.99 |5, -1\rangle \quad \text{in the } |F, m_F\rangle \text{ basis}$$

Hence, for convenience, we refer to these states by the dominant term in the $|F, m_F\rangle$ basis (i.e. $|4, -2\rangle$ and $|5, -1\rangle$ in the example above). The $\Delta F \Delta m_F = +1$ and $\Delta F \Delta m_F = -1$ CTs are each transitions between one state of the first Landau-Zener crossing to a second state of the second crossing, forming a 4-dimensional subspace of the Hilbert space (Figure 1B).

For non-integer [integer] values of I , there are $I + 1/2$ [I] Landau-Zener anticrossings and consequently $2(I - 1/2)$ [$2I$] ESR-type CTs. The minimum complexity required is thus a nuclear spin $I \geq 1$ to have at least two pairs of hyperfine coupled states, which is not the case for phosphorus donors (^{31}P has $I = 1/2$).

Arsenic (^{75}As , $I = 3/2$) and antimony (^{121}Sb , $I = 5/2$ and ^{123}Sb , $I = 7/2$) have sufficient nuclear spin to permit ESR-type CTs, however the hyperfine coupling is relatively weak ($A \sim 198, 186$ and 101 MHz, respectively), so the avoided crossings are found at low magnetic field and transition frequencies (see Table I). Bismuth ^{209}Bi with $I = 9/2$ and $A = 1.475$ GHz is thus the optimal Group V donor in silicon from the point of view of CTs, possessing four of them at GHz frequencies.

	^{75}As ($I = 3/2$)	^{121}Sb ($I = 5/2$)		^{123}Sb ($I = 7/2$)			^{209}Bi ($I = 9/2$)			
$\Delta F = +1, m_F =$	$-1 \leftrightarrow 0$	$-1 \leftrightarrow 0$	$-2 \leftrightarrow -1$	$-1 \leftrightarrow 0$	$-2 \leftrightarrow -1$	$-3 \leftrightarrow -2$	$-1 \leftrightarrow 0$	$-2 \leftrightarrow -1$	$-3 \leftrightarrow -2$	$-4 \leftrightarrow -3$
Magnetic field (mT)	3.8	3.4	10.4	1.8	5.5	9.3	26.6	79.8	133.3	187.8
Frequency (GHz)	0.384	0.552	0.482	0.403	0.376	0.314	7.338	7.032	6.372	5.214

TABLE I. **Summary of ESR-type magnetic-field CTs in donors in silicon.** CTs exist in pairs ($\Delta F \Delta m_F = \pm 1$) separated by less than 0.15 mT in magnetic field and 3 MHz in frequency. Phosphorus does not possess any CT due to its small nuclear spin ($I = 1/2$).

As $df/dB \rightarrow 0$, the next figure of merit is the electron transition probability amplitude, which is always 50% of the high field limit for ESR-types. This means that manipulation times are only slightly reduced while electron coherence times T_{2e} are drastically increased.

Conversely, as flip-flops between two donor electron spins follow the square of this probability amplitude, the flip-flopping rate remains strong, limiting T_{2e} as observed and explained in the main text.

NMR-type CTs occur at strong magnetic field (in Si:Bi, $0.3 \text{ T} < B_0 < 5 \text{ T}$, from $m_I = -9/2$ at low field to $m_I = 9/2$ at high field) and as such are transitions between quasi-pure states in the (m_S, m_I) basis. NMR-type CTs possess a change in nuclear spin state of $\Delta m_I = 1$ and can be manipulated in a conventional electron nuclear double resonance (ENDOR) or NMR experiment. Amongst the NMR-type CTs, those at higher magnetic fields have a smaller electron spin component. This leads to a reduced coupling to the environment, but also increased spin manipulation times, converging to that of a regular NMR transition (typically $\sim 10 \mu\text{s}$).

S2. DECOHERENCE MECHANISMS

Experimental studies of decoherence of donors in silicon have been mostly realized with phosphorus donors. For electron spin coherence, this system represents fairly well the ideal theoretical case of a pure spin-1/2. On the other hand, bismuth measurements here are done mainly in the coupled electron-nuclear spin basis $|F, m_F\rangle$ which, in addition to the high number of nuclear spin states, take this system far from the ideal case. In order to extend spin-1/2 results to the case of bismuth and anticipate the dependence in df/dB , we consider what happens when we measure a specific transition. Considering only S_z types of interaction to a first approximation, the Hamiltonian in the rotating frame of that transition can be simplified to:

$$H_{transition} = \frac{df}{dB} \Delta B_0 S'_z \quad (1)$$

where S' is a spin-1/2 operator and ΔB_0 corresponds to an effective magnetic field variation (first order) from the static field that defines the rotating frame. This simplification is possible as $S_z S_z$ interactions will not take the initial state out of that Hilbert subspace. In the case of flip-flops, it is more complex as nuclear transitions or even the $\Delta F \Delta m_F = -1$ transitions can take this state out of the subspace if a nearby donor has the right spin state. Certain decoherence mechanisms can be considered as effective magnetic field fluctuations, as measured by a ‘central spin’. We treat instrumental magnetic field noise and spectral

diffusion from nuclear spins in the same way, as general fluctuation in magnetic field $\Delta B_z(t)$. (This is an approximation, as spectral diffusion from nuclear spins is affected by the state of the electron spin, and a full treatment of this process is given in Ref [6].) In addition, we consider dipolar coupling to a neighbour donor electron spin, such that overall:

$$\Delta B_0 = \Delta B_z(t) + \sum_i D_i S_{i,z} \quad (2)$$

where D_i is the dipolar interaction strength to neighbour spin S_i .

In Figure 2B of the main text, we assigned the dependence in df/dB to three mechanisms: instantaneous diffusion (ID), indirect and direct flip-flops (iFF and dFF).

ID has been solved [7] using a Markovian method for ensemble averaging between spin-1/2 systems. As it involves two donors with states that are both affected by the resonant microwave excitation, the dipolar interaction term D_i also follows df/dB . As such, df/dB can be thought of as both the sensitivity to magnetic field and the dipolar strength. The ID component (Figure 2A) can thus be derived directly by an appropriate adjustment to the standard equation for a spin-1/2:

$$\frac{1}{T_{\text{ID}}} = C \cdot \left(2\pi \frac{df}{dB} \right)^2 \cdot \frac{\pi}{9\sqrt{3}} \mu_0 \hbar \quad (3)$$

where the normal electron gyromagnetic ratio γ_e was replaced with df/dB and C is the effective spin concentration (1/10th of the actual donor concentration in Bi) [8].

For the case of indirect flip-flops, neighbour spins are still coupled through $S'_z S_{i,z}$ interactions to the central donor, but unlike the case of the ID mechanism, the neighbours may be in any state in the 20-dimensional Hilbert space of Si:Bi, and hence not necessarily at a CT. Both the coupling strength of the central donor spin to the neighbour, as well as expected fluctuation rate in the neighbour spin state from flip-flops cannot be readily calculated: these depends on df/dB of each allowed electron spin transition, their transition probability for flipping and finally detuning between the spins. This neighbour spin detuning is itself a function of df/dB as well as df/dA . However, taking an average over all possible transitions means that the intensity of these fluctuations will remain mostly constant when sweeping magnetic field across the CT. The experimental data were thus modelled to a linear dependence in df/dB , separately for each concentration (Figure 2B). We note that *any* magnetic field fluctuation also produces a linear dependence in df/dB , however the fact that the magnitude of this linear component in our measurements follows the donor

concentration, leads us to conclude that indirect flip-flops are the dominant contribution (this is reasonable, as nuclear spin spectral diffusion is expected to be negligible in these isotopically enriched 28-silicon samples).

Finally, the model for direct flip-flops is very similar to the case described above, however it does not follow at all df/dB as the interaction is of the type $S_x S_x + S_y S_y$. As above, we treat decoherence due to direct flip-flops as a constant, separately for each concentration (Figure 2C). Going beyond this basic model would require full donor-bath simulation such as cluster correlation expansion [6, 9].

In Figure 2B of the main text, each decoherence mechanism is shown separately as a dotted line, and the combined rate is shown as solid curves which plot:

$$\frac{1}{T_2} = \frac{1}{T_{2,ID}} + \frac{1}{T_{2,iFF}} + \frac{1}{T_{2,dFF}} \quad (4)$$

Following the arguments above, the dependence of these rates on df/dB can be expressed as:

$$\frac{1}{T_2} = k_{ID} \left(\frac{df}{dB} \right)^2 + k_{iFF} \left(\frac{df}{dB} \right) + k_{dFF}, \quad (5)$$

where different rate parameters k_i are used when fitting the data from various spin concentrations, as shown in Figure 2.

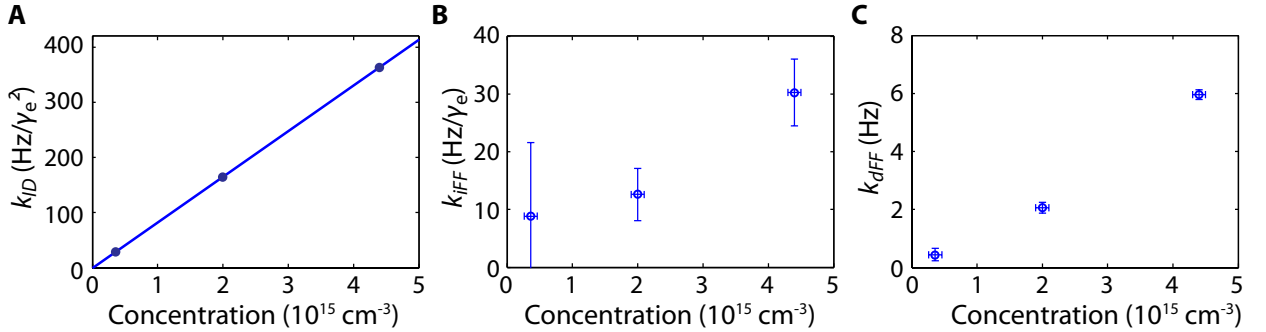


FIG. 2. Parameters used in fitting the data of decoherence vs df/dB , illustrating the dependence of each decoherence mechanism on donor concentration. **A**, k_{ID} was directly computed using equation 3, which dictates a linear dependence of ID on concentration, and was not a free fitting parameter. **B**, k_{iFF} was a fitting parameter, and its dependence on concentration supports our assumption that the primary decoherence mechanism which is proportional to df/dB is due to indirect flip-flops. **C**, k_{dFF} was also a fitting parameter. In these plots, both k_{ID} and k_{iFF} are normalised using the gyromagnetic ratio of a free electron, γ_e .

S3. ESR LINEWIDTHS

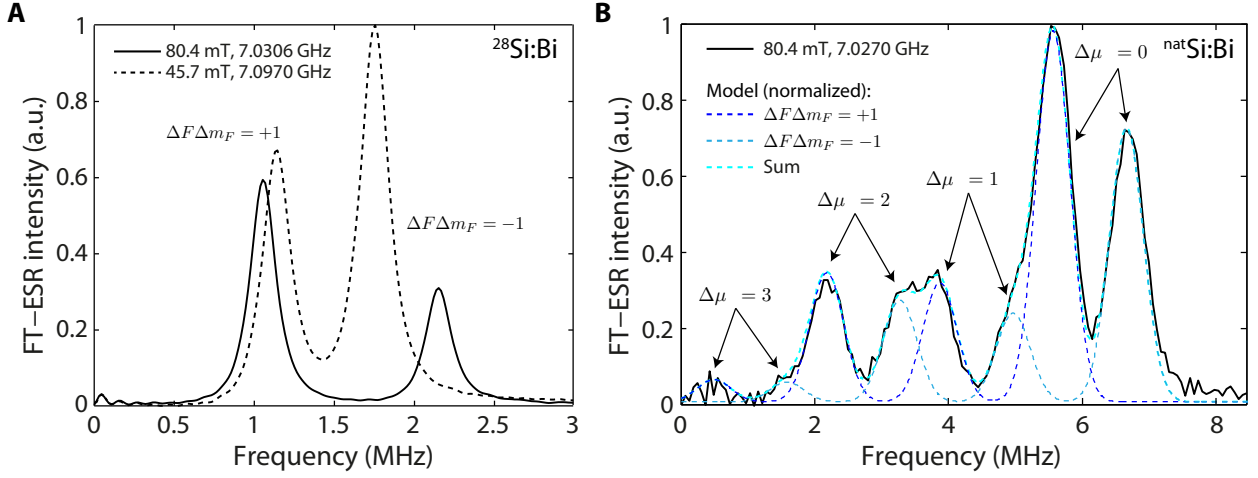


FIG. 3. **FT-ESR around the CT.** Each spectrum is the FT of the free induction decay taken using a microwave frequency slightly below resonance (values given in legend). **A**, For the case of $^{28}\text{Si}:\text{Bi}$, we observe two peaks in the ESR spectrum around the CT, corresponding to the transitions $\Delta F\Delta m_F = \pm 1$. Spectra are shown as measured at two settings of magnetic field/microwave frequency. In the magnetic field domain, the ESR linewidths in these two cases are 1.6 mT close to the CT and 0.07 mT farther away (see Figure 1 of the main manuscript), however in the frequency domain as shown above, the ESR linewidths are constant. **B**, In $^{\text{nat}}\text{Si}:\text{Bi}$, these two primary ESR transitions are further split into sub-peaks, corresponding to a mass-effect from nearest neighbour Si atoms. Each shift of one neutron mass ($\Delta\mu$) yields a shift of -1.7 MHz in transition frequency (or 0.024% change in the hyperfine coupling A). Dashed lines show simulated peaks whose intensity is calculated from a trinomial distribution of ^{30}Si , ^{29}Si and ^{28}Si isotopes in $^{\text{nat}}\text{Si}$ (with respective concentration 3.1%, 4.7% and 92%). As the FT-ESR is derived from the free induction decay, the intensities are normalized by the FT of the inhomogeneous decay T_{2e}^* (Lorentzian) and the cavity bandwidth.

Measurements of spin linewidths provide important details regarding the spin environment, yielding information on crystalline defects and strains amongst other properties. Line broadening arises from a variation in either the hyperfine interaction (ΔA) or the magnetic field (ΔB) (or g-tensor) across the sample. They can either be measured in a magnetic

field-swept spectrum where (to first order):

$$\Delta B_{Total} = \Delta B + \frac{dB}{df} \frac{df}{dA} \Delta A \quad (6)$$

or in Fourier-Transform (FT) ESR where the FT of the free induction decay after a $\pi/2$ rotation gives the spectrum in the frequency domain. In this case, (to first order):

$$\Delta f = \frac{df}{dB} \Delta B + \frac{df}{dA} \Delta A \quad (7)$$

At the CT where $dB/df \rightarrow \infty$, the linewidth in the magnetic field domain broadens strongly until it becomes limited by the second order dependence on magnetic field. Both ΔB and ΔA can be identified by varying the transition frequency and fitting numerically knowing $\frac{dB}{df} \frac{df}{dA}$. To confirm that this change in linewidth is strictly related to the term df/dB , we can make use of the FT ESR technique which simplifies at the CT to $\Delta f = \frac{df}{dA} \Delta A$, where df/dA is quasi-constant around the CT. In Figure 3A, the linewidth is indeed constant about 270 kHz.

In natural silicon, the elimination of the ΔB term dramatically reduces the ESR linewidth. Away from the CT (e.g. at X-band), ΔB is normally around 4 G due to unresolved coupling to ^{29}Si nuclear spins. In the frequency domain, this would be equivalent to nearly 12 MHz, hiding multiple spectral features. First, the two transitions $\Delta F \Delta m_F = \pm 1$ would not be resolvable. Second, as show in Figure 3B, we observe several other peaks (absent in isotopically pure ^{28}Si samples) which arise from variations in the hyperfine coupling due to the total mass of nearest-neighbour silicon atoms (^{28}Si , ^{29}Si and ^{30}Si). This effect is described in full detail, including ENDOR experiments, in a forthcoming work [10].

S4. HYPERFINE CONSTANT ESTIMATION

At a CT, the transition frequency becomes quasi-independent from variations in the static magnetic field B_0 , but more generally from variations in the electron and nuclear Zeeman energies ($\gamma_e B_0$ and $\gamma_n B_0$, respectively). That is why the transition frequency is mainly dependent on the hyperfine constant A , which can be thus estimated with good accuracy.

The value of the hyperfine constant was fitted using least mean squares regression over the measured spectra of $\Delta F \Delta m_F = \pm 1$ around the CT. γ_e was constrained (using the value from [11]) as the uncertainty is much higher at the low magnetic field of the CT. γ_n ,

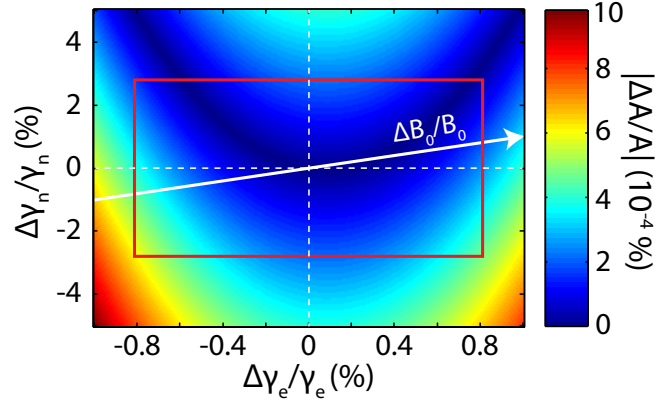


FIG. 4. **Uncertainties in certain Hamiltonian parameters, relevant for the estimation of A .** This figure shows the relative error in the hyperfine constant as a function of relative error in electron (γ_e) or nuclear (γ_n) gyromagnetic ratio. Errors in the static magnetic field B_0 correspond to equal relative changes in both γ_e and γ_n , as shown by the arrow. The red box summarizes the extent of experimental uncertainties.

the nuclear gyromagnetic ratio, was simultaneously fitted with A as no value for γ_n has been reported for Si:Bi with good accuracy. We estimate a possible miscalibration of our magnetic field of up to 0.6 mT; the regression was realized for various values of B_0 giving a final estimation of $A = 1.475169(7)$ GHz and $\gamma_n = 6.9(2)$ MHz/T. The sensitivity of A to these errors is reported in Figure 4. Finally, the small error in mean value of A is mitigated by the known distribution of hyperfine of $\Delta A \approx 60$ kHz across the sample, attributed to lattice strains.

The good accuracy in γ_n may seem slightly surprising considering this highly mixed regime. However, it can be noticed that the difference in transition frequency between $\Delta F \Delta m_F = +1$ and $\Delta F \Delta m_F = -1$ is exactly $2\gamma_n B_0$, independent of A or γ_e . Consequently, the simultaneous fitting of these two transition frequencies offers this higher accuracy.

S5. ELECTRIC FIELD CLOCK TRANSITIONS

In the experiments reported in the main text, CTs were used to reduce the sensitivity of electron spin to magnetic field variations, as quantified by df/dB . While magnetic field noise is indeed the main decoherence mechanism in bulk materials, this may not be the case

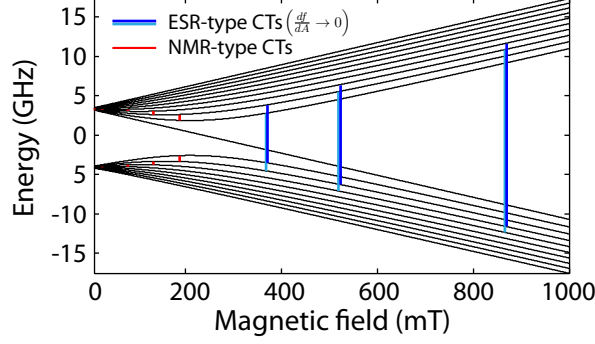


FIG. 5. **Clock transitions in Si:Bi where $df/dA = 0$ which should be robust to electric field noise.** Both ESR- and NMR-type CTs can be observed, as for magnetic-field CTs. One further ESR-CT is found at higher magnetic fields (2.6 T, not shown).

	^{75}As ($I = 3/2$)	^{121}Sb ($I = 5/2$)		^{123}Sb ($I = 7/2$)			^{209}Bi ($I = 9/2$)			
$\Delta m_S = +1, m_I =$	-1/2	-1/2	-3/2	-1/2	-3/2	-5/2	-1/2	-3/2	-5/2	-7/2
Magnetic field (mT)	53	117	39	114	38	23	2607	868	519	369
Frequency (GHz)	1.43	3.21	0.92	3.17	0.98	0.49	72.64	23.18	12.57	7.30

TABLE II. **Summary of ESR-type electric-field CTs in donors in silicon.** At the given magnetic fields, the electron and nuclear spins are weakly coupled and the eigenstates must thus be expressed in the $|m_S, m_I\rangle$ basis. The $[\Delta m_S = \pm 1, \Delta m_I = \mp 2]$ ($\Delta F \Delta m_F = -1$) transitions are nearly completely forbidden here; they would have been found at the same magnetic field as the $[\Delta m_S = \pm 1, \Delta m_I = 0]$ ($\Delta F \Delta m_F = +1$) transitions, but separated by less than 40 MHz in frequency.

in nanoscale devices where the electric field at interfaces could couple strongly with both the donor electron and nuclear spins through the hyperfine interaction (and also, to lesser extent, through a modulation in the electron spin g-factor). The sensitivity of a spin to this effect can be quantified by the gradient of the frequency with respect to the hyperfine constant df/dA , combined with values for the DC Stark effect for donors in silicon (which for Group V donors is in the order of $10^{-3} \mu\text{m}^2/\text{V}^2$, as a fractional change in the hyperfine coupling [12, 13]). Those CTs which will be most robust to electric field noise ($df/dA \rightarrow 0$) are identified in Si:Bi in Figure 5 and in Table II for all Group V donors in silicon.

In practice, both magnetic and electric field fluctuations will participate to the donor spin

decoherence. There will thus be an optimal CT, at a specific magnetic field and frequency, where the coherence time would be maximum. For example, the magnetic field CT near 188 mT in Bi has the lowest value of df/dA out of the four possible CTs. In other scenarios, it might be advantageous to minimise the inhomogeneous broadening as much as possible (e.g. for coupling a spin ensemble to a microwave resonator), and this would also require different optimal operating points within the Hilbert space of the bismuth electron and nuclear spins.

* gary.wolfowicz@materials.ox.ac.uk

† jjl.morton@ucl.ac.uk

- [1] Mohammady, M. H., Morley, G. W. & Monteiro, T. S. Bismuth Qubits in Silicon: The Role of EPR Cancellation Resonances. *Phys. Rev. Lett.* **105**, 067602 (2010).
- [2] Mohammady, M. H., Morley, G. W., Nazir, A. & Monteiro, T. S. Analysis of quantum coherence in bismuth-doped silicon: A system of strongly coupled spin qubits. *Phys. Rev. B* **85**, 094404 (2012).
- [3] Hardy, W., Berlinsky, A. & Whitehead, L. Magnetic Resonance Studies of Gaseous Atomic Hydrogen at Low Temperatures. *Phys. Rev. Lett.* **42**, 1042-1043 (1979).
- [4] Longdell, J., Alexander, A. & Sellars, M. Characterization of the hyperfine interaction in europium-doped yttrium orthosilicate and europium chloride hexahydrate. *Phys. Rev. B* **74**, 195101 (2006).
- [5] Steger, M. *et al.* Optically-detected NMR of optically-hyperpolarized ^{31}P neutral donors in ^{28}Si . *J. App. Phys.* **109**, 102411 (2011).
- [6] Balian, S. J. & Monteiro, T. S. Theoretical analysis of spin qubit decoherence near optimal working points. *arXiv preprint* 1302.1709 (2013).
- [7] Salikhov, K., Dzuba, S. & Raitisimring, A. The theory of electron spin-echo signal decay resulting from dipole-dipole interactions between paramagnetic centers in solids. *J. Mag. Res.* **42**, 255276 (1981).
- [8] Wolfowicz, G. *et al.* Decoherence mechanisms of ^{209}Bi donor electron spins in isotopically pure ^{28}Si . *Phys. Rev. B* **86**, 245301 (2012).
- [9] Witzel, W., Carroll, M., Cywinski, L. & Das Sarma, S. Quantum decoherence of the central

- spin in a sparse system of dipolar coupled spins. *Phys. Rev. B* **86**, 035452 (2012).
- [10] Tyryshkin, A. M. *et al.*, in preparation (2013).
- [11] Feher, G. Electron spin resonance experiments on donors in silicon. I. Electronic structure of donors by the electron nuclear double resonance technique. *Phys. Rev.* **114**, 12191244 (1959).
- [12] Bradbury, F. *et al.* Stark Tuning of Donor Electron Spins in Silicon. *Phys. Rev. Lett.* **97**, 176404 (2006).
- [13] Rahman, R. *et al.* High Precision Quantum Control of Single Donor Spins in Silicon. *Phys. Rev. Lett.* **99**, 036403 (2007).